Earth, Planets and Space

EXPRESS LETTER

Open Access

Discrete aurora and the nightside ionosphere of Mars: an EMM–MEX conjunction of FUV imaging, ionospheric radar sounding, and suprathermal electron measurements

Yuki Harada[1*], Yuka Fujiwara[1], Robert J. Lillis[2], Justin Deighan[3], Hiromu Nakagawa[4], Beatriz Sánchez-Cano[5], Mark Lester[5], Yoshifumi Futaana[6], Mats Holmström[6] and Rudy A. Frahm[7]

Abstract

Since 2021, a new surge in discrete aurora detections at Mars has been observed by the Emirates Mars Ultraviolet Spectrometer (EMUS) onboard the Emirates Mars Mission (EMM) Hope Orbiter as EMUS started to regularly obtain synoptic auroral images with a high sensitivity. Here we report on a fortuitous conjunction between EMM and Mars Express (MEX) using far ultraviolet (FUV) imaging of discrete aurora by EMM EMUS, in situ measurements of suprathermal electrons by the MEX Analyzer of Space Plasma and Energetic Atoms Electron Spectrometer (ELS), and topside radar sounding of the nightside ionosphere by the MEX Mars Advanced Radar for Subsurface and Ionosphere Sounding (MARSIS). In this event, EMM EMUS imaged a clear discrete aurora signature around moderately strong crustal magnetic fields on the nightside near the dusk terminator, 11 min before which MEX MARSIS measured a prominent local enhancement of the peak electron density in the nightside ionosphere and MEX ELS observed an in situ enhancement of suprathermal electrons at the corresponding location. A remarkable geographic agreement is found between the enhancements of the aurora, ionosphere, and suprathermal electrons, suggesting that the enhanced ionization and auroral emission are caused concurrently by precipitating suprathermal electrons. Subsequent images indicate that the discrete aurora slightly changed its shape in 15 min and mostly disappeared in a few hours. The MEX MARSIS measurements of the auroral ionosphere display overlapping ionospheric and surface echoes indicative of horizontal gradients of the peak electron density. Analysis of the overlapping echoes implies that the auroral ionosphere and electron precipitation could be highly structured with horizontal spatial scales on the order of several tens of km. MEX MARSIS also observed a non-auroral ionospheric enhancement with a wider spatial extent than the local auroral enhancement, suggesting alternative sources of the enhanced nightside ionosphere such as plasma transport. The comparison between the ionospheric structures measured by MEX MARSIS, suprathermal electron flux measured by MEX ELS, and discrete auroral emission imaged by EMM EMUS underscores the complexity of the auroral and non-auroral nightside ionospheres. This motivates further investigations of their sources, transport, and connections to the magnetotail dynamics of Mars.

Keywords Mars, Discrete aurora, Ionosphere, FUV, Radar, EMM, Mars Express

*Correspondence:
Yuki Harada
haraday@kugi.kyoto-u.ac.jp
Full list of author information is available at the end of the article

Graphical Abstract

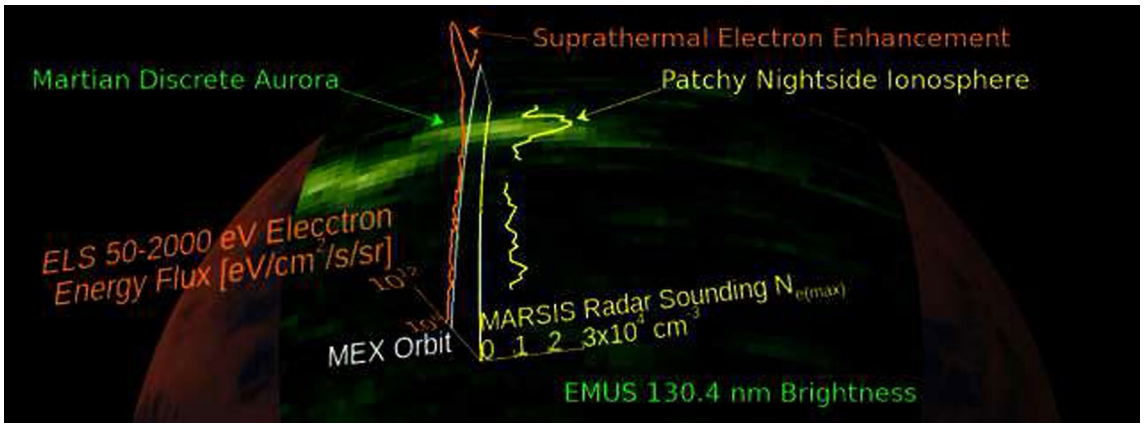

Introduction

Since the discovery of aurora at Mars (Bertaux et al. 2005), observations and modeling of the Martian aurora have continued to shed light on the interplay between the upper atmosphere and the space environment of Mars. Among the different types of the Martian aurora (Schneider et al. 2015, 2018; Deighan et al. 2018; Ritter et al. 2018; Chaffin et al. 2022), discrete aurora at Mars represents spatially and temporally confined auroral emission conventionally observed in the crustal magnetic fields of Mars (Acuña et al. 1999) and is typically interpreted as driven by suprathermal electron precipitation (Leblanc et al. 2006, 2008; Brain and Halekas 2013; Gérard et al. 2015; Soret et al. 2016, 2021; Schneider et al. 2021). The occurrence of discrete aurora in the strong crustal field region (60°S–30°S, 150°E –210°E) shows clear dependence on the local time and the polarity of the interplanetary magnetic field (IMF) B_y component (Schneider et al. 2021), while the auroral occurrence outside the strong crustal field region depends strongly on the solar wind dynamic pressure (Girazian et al. 2022). These statistical trends are favorably compared with in situ observations of auroral electrons with energies of 50–2000 eV (Brain et al. 2006; Xu et al. 2020, 2022a). The local-time and IMF-B_y dependences of the auroral occurrence in the strong crustal field region can be explained in terms of magnetic reconnection between the draped IMF and crustal magnetic fields (Johnston et al. 2023; Bowers et al. 2023a). Most recently, high-sensitivity and wide-coverage observations by the Emirates Mars Mission (EMM) Emirates Mars Ultraviolet Spectrometer (EMUS) have started unraveling new aspects of the Martian discrete aurora, including their prevalence, instantaneous morphology, temporal evolution, and additional categories including the non-crustal field patchy aurora and "sinuous" aurora (Lillis et al. 2022). These observations suggest a close connection between the discrete aurora and magnetotail dynamics at Mars, the latter of which (a) controls the magnetic field lines guiding suprathermal electrons to the atmosphere and (b) potentially drives the acceleration processes of auroral electrons. The dynamically changing shapes and patterns of the discrete aurora of Mars are likely driven by a variety of dynamic processes that are known to operate in the Martian magnetotail (e.g., Dubinin and Fraenz 2015; Halekas et al. 2021). To name a few, in situ particle and field measurements have revealed the presence of magnetic reconnection (Eastwood et al. 2008, 2012; Halekas et al. 2009; Harada et al. 2015, 2017, 2020; Hara et al. 2017; Wang et al. 2023), energy-dispersed ions and electrons (Halekas et al. 2015; Harada et al. 2016a; Zhang et al. 2023a), tail current sheet flapping (DiBraccio et al. 2015, 2017; Zhang et al. 2023b), and plasma waves (Espley et al. 2004, 2005; Ruhunusiri et al. 2015; Harada et al. 2016b, 2019; Fowler et al. 2021; Teng et al. 2023) in the magnetotail of Mars.

Until recently, the nightside ionosphere of Mars was a relatively unexplored region as opposed to the extensively studied dayside ionosphere (e.g., Withers 2009). In the absence of photoionizing solar radiation, the primary sources of the Martian nightside ionosphere can be either electron impact ionization or transport from the dayside ionosphere (e.g., Fox et al. 1993). Radar sounding by the Active Ionospheric Sounding mode of the Mars Advanced Radar for Subsurface and

Ionosphere Sounding (MARSIS) onboard Mars Express (MEX) and radio occultation observations by the Mars Express Radio Science Experiment indicate that the Martian nightside ionosphere is patchy and sporadic, exhibiting spatial inhomogeneity often associated with the crustal magnetic field distribution and temporal variability in response to the changing upstream solar wind conditions and space weather events (Safaeinili et al. 2007; Gurnett et al. 2008; Němec et al. 2010, 2011, 2014; Withers et al. 2012; Duru et al. 2011; Cartacci et al. 2013; Diéval et al. 2014; Harada et al. 2018a; Qin et al. 2021; Lester et al. 2022). In situ observations by the Mars Atmosphere and Volatile Evolution (MAVEN) mission provide a wealth of information on the nightside ionosphere such as the ion composition, global and local structures, seasonal and long-term variability, and species-by-species response to the suprathermal electron precipitation (Fowler et al. 2015; Girazian et al. 2017a, b, 2021; Adams et al. 2018; Cui et al. 2019; Mayyasi et al. 2019; Qin et al. 2022; Xu et al. 2022b). Despite the growing body of knowledge derived from these observations, the relationship between the spatiotemporal variability of the nightside ionosphere and the magnetotail dynamics at Mars remains poorly understood.

In this letter, we present a fortuitous conjunction of topside radar sounding of the Martian nightside ionosphere by MEX MARSIS, suprathermal electron measurements by the Analyzer of Space Plasma and Energetic Atoms (ASPERA-3) Electron Spectrometer (ELS) (Barabash et al. 2006) also onboard MEX, and far ultraviolet (FUV) imaging of discrete aurora by EMM EMUS. The

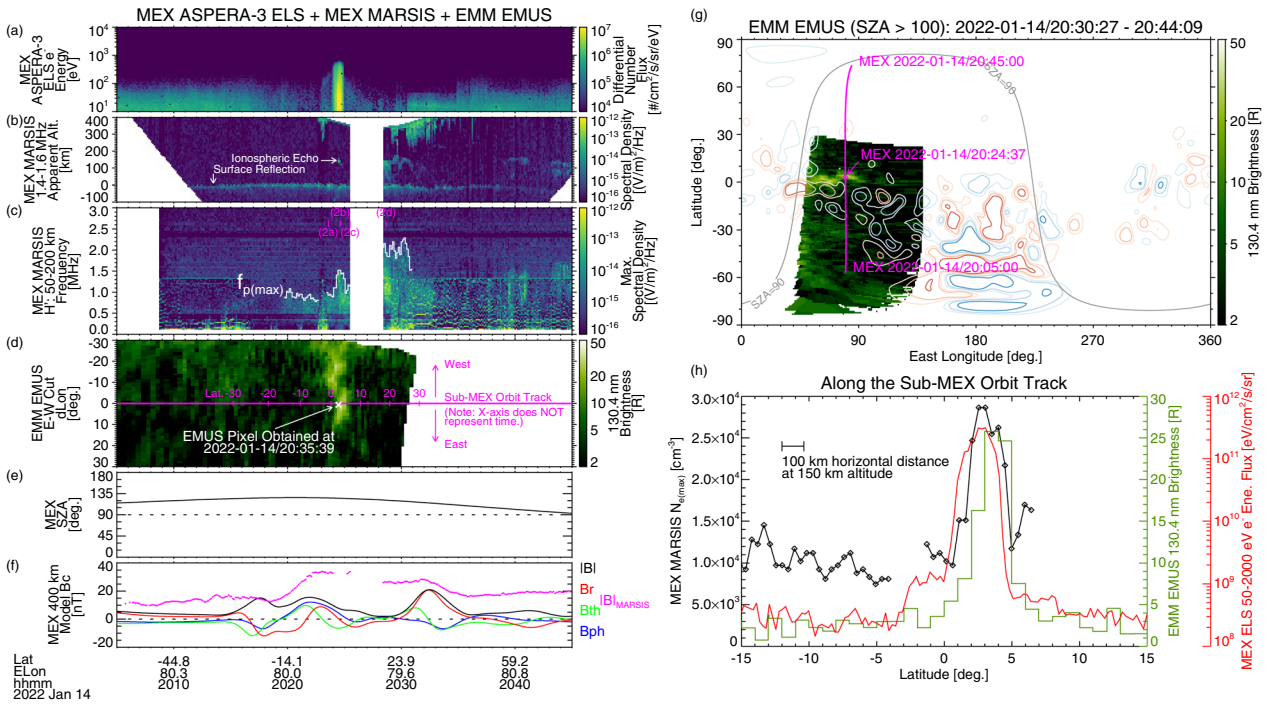

Fig. 1 Overview of the EMM–MEX conjunction event of discrete aurora observations at Mars. **a** Energy–time spectrogram of suprathermal electrons obtained by MEX ASPERA-3 ELS. MEX MARSIS echo intensities as a function of **b** apparent altitude and time (radargram) showing the average intensity in a frequency range of 1.4-—1.6 MHz and **c** radio frequency and time (spectrogram) showing the maximum intensity in an apparent altitude range of 50–200 km along with the maximum plasma frequency ($f_{p(max)}$) of the ionospheric echo denoted by the white lines. The magenta labels of "(2a)"–"(2d)" indicate the acquisition timings of the ionograms shown in Fig. 2. **d** EMM EMUS 130.4 nm brightness around the sub-MEX orbit track. Note that the horizontal axis in this panel corresponds to the MEX latitude and does not represent time. **e** MEX solar zenith angle. **f** Crustal magnetic field at the MEX longitude and latitude at a 400 km altitude computed from Morschhauser et al. (2014)'s model. The magenta dots show the magnetic field strength extracted from the electron cyclotron echoes recorded in MARSIS ionograms (Akalin et al. 2010). The latitude and east longitude of MEX are shown along the time axis. **g** Image of 130.4 nm emission obtained by EMM EMUS and the MEX orbit on a geographic longitude and latitude map. The gray curve indicates the solar zenith angle of 90°. The red and blue contours show the outward and inward radial component of the crustal magnetic field at a 400 km altitude computed from Morschhauser et al. (2014)'s model, denoting -40, -20, -10, 10, 20, and 40 nT from blue to red. **h** Zoom-in comparison of the peak electron density ($N_{e(max)}$) measured by MEX MARSIS, the integrated electron energy flux over 50–2000 eV measured by MEX ASPERA-3 ELS, and 130.4 nm emission measured by EMM EMUS as a function of latitude along the sub-MEX orbit track

quasi-simultaneous observations of the peak electron density, suprathermal electrons, and the auroral emission enable us to directly link the nightside ionospheric structures and suprathermal electron precipitation to the two-dimensional visualization of energy deposition from the magnetotail to the upper atmosphere represented by discrete aurora.

Observations

Figure 1 provides an overview of the EMM–MEX conjunction event of discrete aurora on 14 January 2022 (MEX Orbit 22790). MEX conducted active ionospheric sounding and suprathermal electron measurements around the periapsis as it traveled northward on the nightside, passing over moderately strong crustal magnetic fields near the equator (Fig. 1e, f, and g). Figure 1b shows the MEX MARSIS observations during 20:05–20:45 UTC in the radargram format. We observe the horizontal trace around the apparent altitude of 0 km representing reflection from the surface of Mars along with sporadic ionospheric echoes between 0–200 km. These are typical signatures of MEX MARSIS sounding of the nightside ionosphere (Němec et al. 2010, 2011; Diéval et al. 2014). Figure 1a shows in situ measurements of suprathermal electrons by MEX ASPERA-3 ELS in the same time interval, indicating a distinct enhancement of local suprathermal electron flux during 20:24–20:25 UTC as discussed in detail later in this section. Meanwhile, EMM EMUS obtained a raster-scanned image from 20:30:27 to 20:44:09 UTC as shown in Fig. 1g. Here we derive the 130.4 nm brightness by integrating differential radiance in a wavelength range of 129–132 nm and generate a geographic emission map of a $1^\circ \times 1^\circ$ resolution by averaging contributions from overlapping pixels in a similar manner to Lillis et al. (2022). As we are interested in auroral emission, we only show nightside pixels obtained at $> 100^\circ$ solar zenith angles. In Fig. 1g, we observe a clear discrete aurora signature around 0° latitudes and 50°E–90°E longitudes extending from the dusk terminator. The auroral emissions are located around the moderately strong crustal magnetic fields but appear to be offset from the radial field region as sometimes seen for "crustal field aurora" near the dusk terminator (Lillis et al. 2022). As shown by the MEX orbit track in Fig. 1g, MEX traveled directly above the discrete aurora. A detailed investigation of the acquisition times of individual pixels indicates that the nearest pixel of the EMM EMUS image to the sub-MEX position on the discrete aurora was taken at 20:35:39 UTC as indicated by the white label in Fig. 1d, only 11 min after MEX MARSIS conducted radar and in situ measurements at the corresponding location at 20:24:37 UTC as labeled in Fig. 1g. The close proximity in time of the MEX MARSIS ionospheric sounding, MEX ELS in situ measurements, and EMM EMUS auroral imaging makes this event an excellent case for a direct comparison between the auroral emission pattern, ionospheric properties, and suprathermal electrons.

Here we briefly examine the surrounding magnetic field conditions of this discrete aurora. As shown in Fig. 1g, the discrete aurora was observed on the dusk-side and located northeast of the radially outward crustal field region (red contours), suggesting a locally northward and eastward crustal field direction (corresponding to "Bth" < 0 and "Bph" > 0 in Fig. 1f). The magenta dots in Fig. 1f indicate the local magnetic field strength at the MEX position estimated from the electron cyclotron echoes recorded in MARSIS ionograms (Gurnett et al. 2008; Akalin et al. 2010). We observe that the local magnetic field exceeds 30 nT around 20:24:37 UTC at the MEX altitude of ~400 km above the discrete aurora. This is significantly stronger than both the model crustal field strength at 400 km altitude (black line in Fig. 1f) and the draped field strength of ~10–20 nT observed at higher altitudes before 20:15 UTC and after 20:36 UTC (magenta dots in Fig. 1f). This implies an enhanced pileup of draped IMF, compression and deformation of crustal fields, or combinations thereof. The upstream solar wind was not directly measured by MAVEN due to the orbit configuration, but the IMF clock angle proxy in the dayside magnetosheath (Dong et al. 2019) infers an IMF condition of generally $+B_y$ and mixed B_z polarities for this event (not shown). Because of the varying IMF clock angle proxy, we cannot make a conclusive statement about the shear angle between the draped IMF and underlying crustal fields (Bowers et al. 2023b) and its implications for magnetic reconnection potentially driving discrete aurora (Johnston et al. 2023; Bowers et al. 2023a).

Figure 1c shows the MEX MARSIS observations in the spectrogram format with a focus on the ionospheric echoes. The enhanced echo intensities over a continuous range of frequencies represent the ionospheric echoes in this format, while the stripe-like patterns arise from local plasma oscillations (e.g., Gurnett et al. 2008) and are not of interest here. The white lines in Fig. 1c mark the upper edge of the ionospheric echo signals, namely the maximum frequency of the ionospheric echoes ($f_{p(max)}$), extracted by examining individual ionograms. Specifically, for a given ionogram, potential signals with spectral densities exceeding 10^{-15} $(V/m)^2/Hz$ are automatically marked by our software. Then, we visually identify an ionospheric echo trace and record the maximum frequency. Some representative ionograms are shown in Fig. 2 with the identified $f_{p(max)}$ of the ionospheric echoes indicated by the white labels. For comparison, east–west cuts of the 130.4 nm emission map around the sub-MEX orbit track are shown in Fig. 1d. Around 20:24:30 UTC,

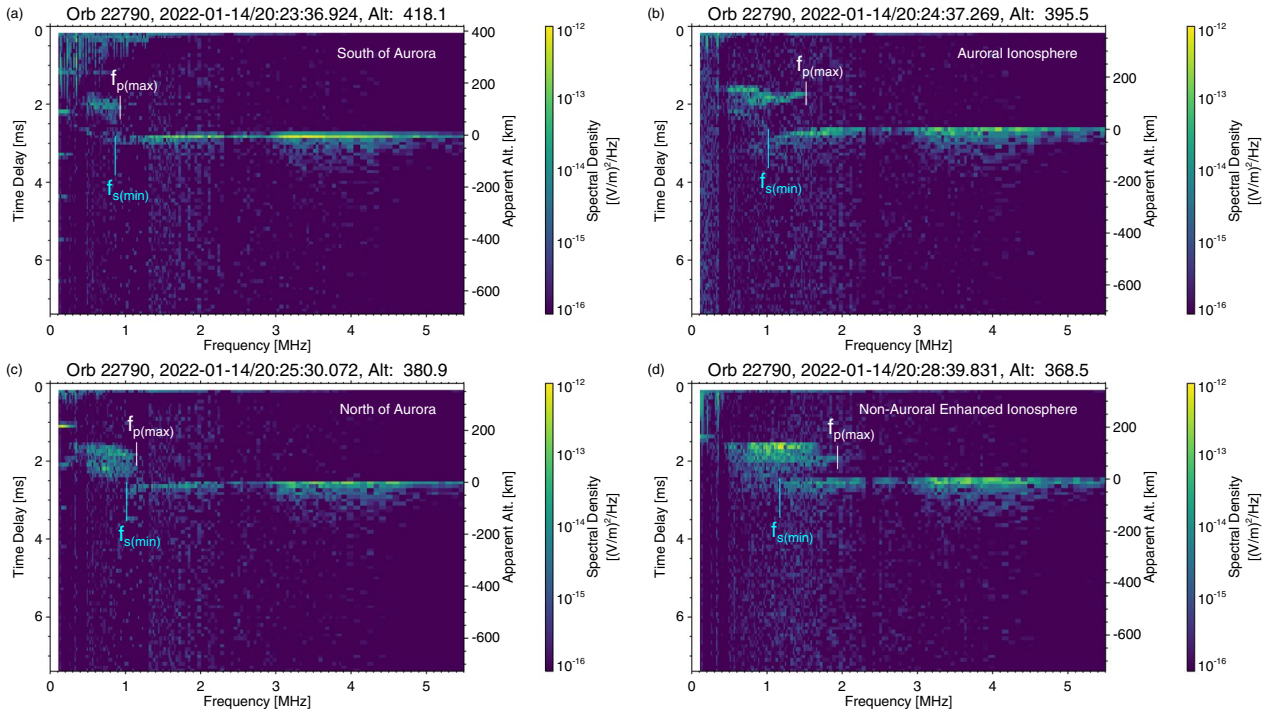

Fig. 2 Representative ionograms obtained by MEX MARSIS. Echo intensity as a function of time delay and radio frequency obtained when MEX was located at **a** south of the discrete aurora, **b** immediately above the discrete aurora, **c** north of the discrete aurora, and **d** distant from the discrete aurora

we observe a sharp enhancement of $f_{p(max)}$ up to 1.5 MHz (Fig. 1c) and intense suprathermal electron fluxes at energies below $\sim$ 600 eV (Fig. 1a) remarkably coinciding with the location of the discrete aurora emission (Fig. 1d). A zoom-in comparison of the radar ionospheric measurements, in situ suprathermal electrons, and FUV auroral emission along the sub-MEX orbit track is shown in Fig. 1h. Here the peak electron density, $N_{e(max)}$, is converted from $f_{p(max)}$ using the relation of $f_p = 8980\sqrt{N_e}$, where f_p is the electron plasma frequency in Hz and N_e is the electron density in cm^{-3}. We observe the enhanced $N_{e(max)}$ of 2.9×10^4 cm^{-3}, which is quite high for the nightside ionosphere of Mars (cf. $N_{e(max)} < 5 \times 10^3$ cm^{-3} for 90% of the time on the nightside as estimated by Němec et al. (2010)). The red line in Fig. 1h shows the integrated electron energy flux over 50–2000 eV, which is used as an empirical measure to select auroral electron events (Xu et al. 2022a). The observed peak energy flux reaches 3.1×10^{11} eV/cm^2/s/sr, far exceeding the empirical threshold of 1.1×10^{10} eV/cm^2/s/sr for auroral emission detectable by MAVEN imaging ultraviolet spectrograph instrument (Xu et al. 2022a). In Fig. 1h, the local enhancements of $N_{e(max)}$ (black), suprathermal electron energy flux (red), and auroral emission (green) overlap with each other for the most part and have similar widths of $\sim$ 3°–4° in latitude corresponding to ~180–250 km in horizontal distance, yet we observe a small $\sim$ 1° shift between the peaks, which will be discussed later in this section. The striking similarity between the enhancements of $N_{e(max)}$, suprathermal electrons, and auroral brightness provides compelling evidence that the enhanced nightside ionosphere is caused by precipitating suprathermal electrons that also give rise to the discrete aurora.

We point out that the nightside ionosphere is also enhanced in a region far from the discrete aurora. Specifically, MARSIS measured consistently high $f_{p(max)}$ of ~2 MHz from 20:28 to 20:31 UTC after the data gap (Fig. 1c) while we observe suprathermal electron depletions (Fig. 1a) and virtually no auroral emission at the corresponding locations (Fig. 1d). Such suprathermal electron depletions observed at altitudes above the electron exobase on the nightside suggest closed magnetic field line topology with both footpoints on the nightside (Mitchell et al. 2001; Brain et al. 2007; Steckiewicz et al. 2015). This non-auroral enhanced ionosphere is observed $\sim$ 15°–25° north of the discrete aurora above a weak crustal magnetic field region (Fig. 1f) with a wider spatial extent compared to the local auroral enhancement. The absence of auroral emission and suprathermal electrons suggest that this ionospheric enhancement is not caused by immediate electron impact ionization by precipitating

electrons, and by elimination, we can infer that plasma transport (e.g., low-altitude ion transport by collisional coupling with neutral winds (Adams et al. 2018)) could be implicated in forming the enhanced nightside ionosphere observed by MARSIS above the weak crustal field region. Alternatively, MEX ELS may have missed suprathermal electron precipitation due to its limited field of view.

We now investigate detailed ionospheric echo properties in the ionograms shown in Fig. 2. Figure 2b shows the ionogram obtained directly above the discrete aurora (see the label "(2b)" in Fig. 1c). A notable feature of this "auroral ionosphere" ionogram is that the maximum frequency of the ionospheric echo, $f_{p(max)}$, is significantly higher than the minimum frequency of the surface echo, $f_{s(min)}$ as opposed to ideal expectation for a horizontally stratified ionosphere for which $f_{p(max)}$ is equal to $f_{s(min)}$. These ionospheric and surface echoes with overlapping frequencies can be explained by a vertically reflected surface echo and an obliquely reflected ionospheric echo from a slant iso-density surface of the ionosphere (Duru et al. 2010). The vertical critical frequency, $f_{s(min)}$, is determined by the peak density at the nadir ionosphere, and the oblique $f_{p(max)}$ is determined by the peak density of the slant reflection surface at the off-nadir ionosphere. In other words, the overlapping ionospheric and surface echoes are indicative of horizontal gradients of the peak electron density. For the ionograms obtained at locations adjacent to the discrete aurora (Figs. 2a and c), the overlapping feature is not as prominent as the auroral ionosphere. The overlapping ionospheric and surface echoes are also observed for the non-auroral enhanced ionosphere (Fig. 2d).

Based on analysis of the ionogram obtained above the discrete aurora (Fig. 2b) and on a geometric consideration of the overlapping ionospheric and surface echoes as shown in Fig. 3, we can estimate the horizontal gradient of the peak electron density of the auroral ionosphere. The observed properties of the presumably oblique ionospheric echo indicate the maximum electron plasma frequency of $f_{p(max)} = 1.52$ MHz and the apparent range to the electron density peak of $R' = 258$ km. Here R' represents the virtual distance to the target under the assumption that the radio wave propagates at the speed of light, and the actual range, R, is smaller than R' because of the dispersion of the radar pulse propagating through the ionized medium with group velocities slower than the speed of light. The observed minimum frequency of the surface echo, $f_{s(min)}$, indicates that the sub-MEX vertical critical frequency is 1.02 MHz. Since the peak altitude of the nightside ionosphere is typically $\sim$ 150 km in the presence of precipitating suprathermal electrons (Fillingim et al. 2007; Lillis et al. 2009; Girazian et al. 2017a), we assume an ionospheric peak altitude of $h_{iono} \sim 150$ km. We note that the peak altitude of Martian discrete aurora is expected to be generally around $\sim$ 135 km (Schneider et al. 2021; Soret et al. 2016, 2021). With these observations and assumptions, the off-nadir angle of the oblique echo, θ, and the horizontal distance from the sub-MEX point to the oblique echo reflection point at the peak altitude, d, can be estimated as $\theta <\sim 18°$ and $d <\sim 80$ km (Fig. 3). This suggests that the overlapping ionospheric and surface echoes result from the peak electron density varying from 1.3×10^4 cm^{-3} to 2.9×10^4 cm^{-3} within a horizontal distance of $<\sim 80$ km. This distance is comparable to, or even smaller than, the effective spatial resolution of the EMM EMUS image (the nearest EMUS pixel to the sub-MEX position at the MARSIS auroral ionospheric measurement has 4.9° longitude $\times$ 0.91° latitude widths, approximately corresponding to 300 km $\times$ 55 km at 150 km altitude), implying that there

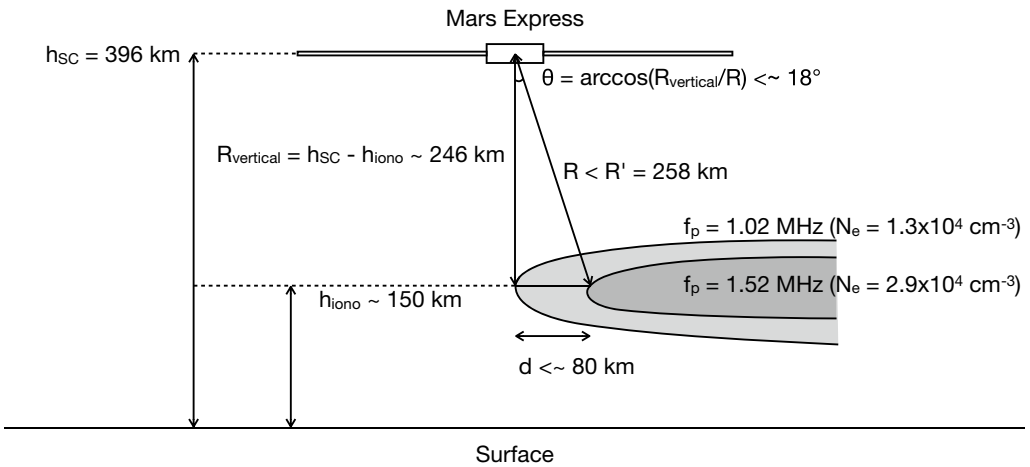

Fig. 3 Schematic illustration of a geometric consideration of the overlapping ionospheric and surface echoes. See text for details

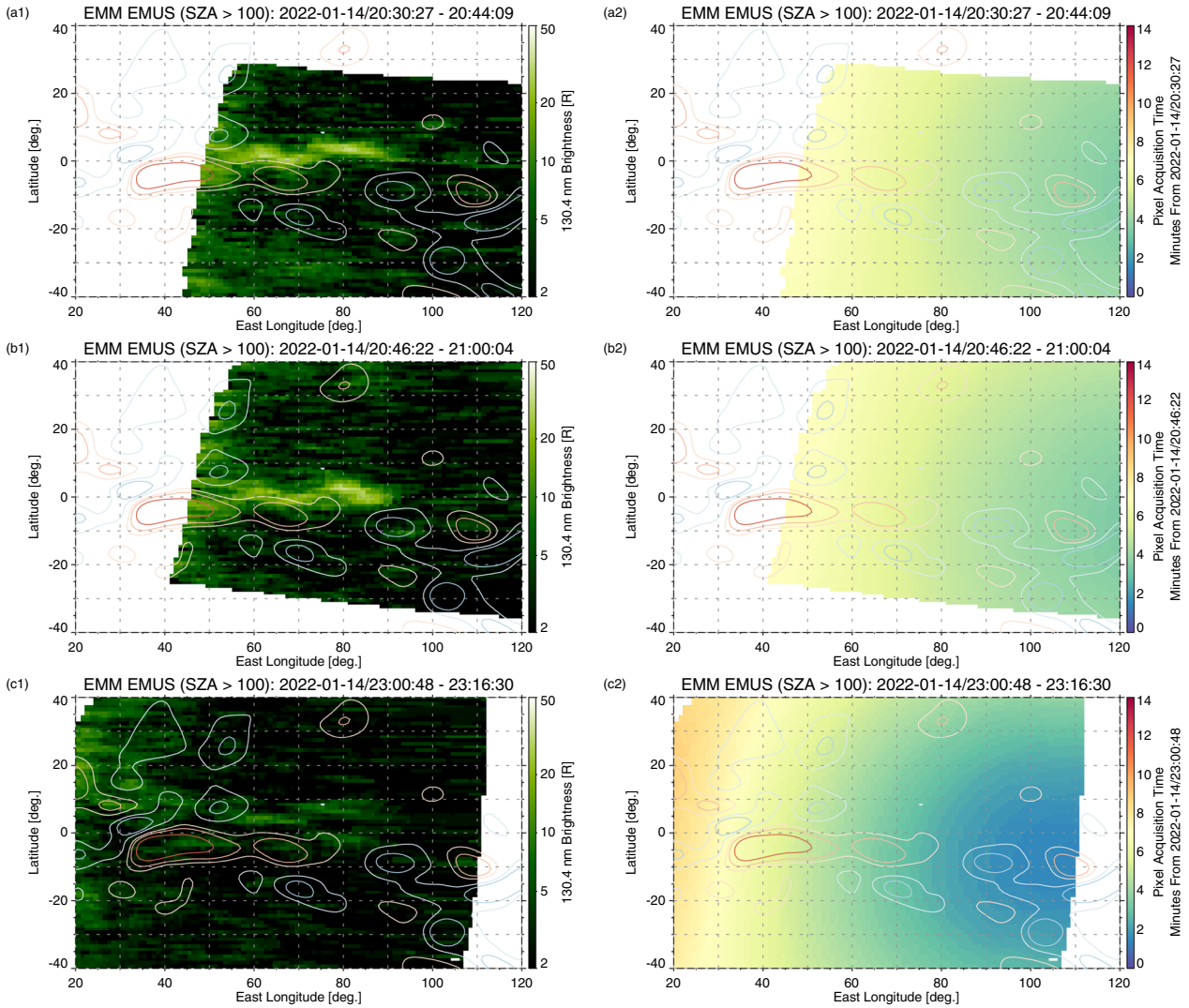

Fig. 4 Images of 130.4 nm emission of the same region taken by EMM EMUS. The images were taken at **a1** ~11 min, **b1** ~26 min, and **c1** ~2.6 h after the MEX MARSIS observation of the peak electron density enhancement. For reference, the times at which individual pixels were measured are indicated in panels (**a2**, **b2**, **c2**)

could be spatial inhomogeneity of aurora unresolved by EMM EMUS for this event.

Another point to note is that the ionospheric echoes recorded in Fig. 2a–d have relatively broad widths in time delay even though the transmitted pulse has a very short duration corresponding to the width of one time-delay bin. These signatures are referred to as "diffuse echoes" in the literature and are interpreted as a superposition of multiple echoes reflected at oblique angles from ionospheric irregularities (Gurnett et al. 2008; Harada et al. 2018b). Diffuse echoes are commonly observed for the nightside ionosphere (Harada et al. 2018b) as expected for generally large fluctuations of electron and ion densities in the nightside ionosphere (Girazian et al. 2017b; Park 2024).

Finally, we examine the time evolution of the discrete aurora by comparing the EMM EMUS images obtained at different times (Fig. 4). Figure 4a1 shows a close-up of the EMM EMUS image shown in Fig. 1g, and 4b1 and 4c1 shows subsequent images of the same region obtained by EMM EMUS available for this event. Figure 4a2, b2, and c2 demonstrates how the pixel acquisition times vary over the maps. The nearest pixels to the sub-MEX position at the MARSIS auroral ionospheric measurement were taken at 20:51:28 UTC for Fig. 4b1 and at 23:03:18 UTC for Fig. 4c1. We can see

that the discrete auroral pattern slightly varies its shape over ~15 min from Fig. 4a1 to Fig. 4b1. Such small yet visible variations on ~10 min time scales may explain the aforementioned small shift between the $N_{e(max)}$ and auroral emission enhancements (the black and green lines in Fig. 1h), which were observed 11 min apart. Also, the in situ measurements of suprathermal electrons at the MEX altitude do not necessarily map exactly to the nadir auroral emission depending on the magnetic field configuration (Qin et al. 2021), which could explain the shift between the enhancements of the suprathermal electrons and auroral emission (the red and green lines in Fig. 1h). In Fig. 4c1 (~2 h later), the overall auroral emission intensity is greatly weakened and the once-coherent structure of clear discrete aurora has fragmented into small patches of very weak emission, suggesting that this discrete aurora pattern had almost disappeared by this time. The dynamics of the Martian discrete aurora could be attributed to temporally varying magnetic field and plasma conditions in the magnetotail resulting from the dynamic solar wind–Mars interaction.

Conclusions and implications

We analyze the quasi-simultaneous FUV, radar, and in situ electron observations relevant to discrete aurora at Mars. In this event, the FUV image of a clear discrete aurora on the duskside of Mars was obtained by EMM EMUS just 11 min after MEX MARSIS conducted topside radar sounding of the nightside ionosphere and MEX ELS measured the enhancement of suprathermal electrons. We observe a local and distinct enhancement of the ionospheric peak electron density (up to 2.9×10^4 cm^{-3}) and in situ electron energy flux (up to 3.1×10^{11} $eV/cm^2/s/sr$ in the 50–2000 eV energy range) spatially coinciding well with the discrete auroral emission, demonstrating that the locally enhanced nightside ionosphere and discrete aurora at Mars are caused by a common agent: precipitating suprathermal electrons. The subsequent auroral images of the same region indicate that the discrete aurora was dynamic, exhibiting time-varying patterns and intensities. The auroral emission slightly changed its shape over 15 min and its overall intensity mostly diminished in a few hours. Based on the properties of the overlapping ionospheric and surface echoes measured by MEX MARSIS, we can infer that the peak electron densities vary by a factor of 2 or more within a horizontal distance of $<\sim$ 80 km. The observed inhomogeneity of the auroral ionosphere suggests that the auroral electron precipitation could be highly structured with horizontal spatial scales on the order of several tens of km. Meanwhile, a broader region of enhanced electron densities was observed with suprathermal electron depletions and without any prominent auroral emission around 15°–25° north of the discrete aurora, implying a non-auroral source of the nightside ionosphere in this region (e.g., plasma transport from the dayside ionosphere via collisional neutral-ion coupling at low altitudes (Adams et al. 2018)). To examine the nightside ionospheric sources, in situ ion composition measurements will be highly informative (Girazian et al. 2017b), and further investigations should be conducted to reveal the sources and behaviors of the non-auroral nightside ionosphere of Mars. Both the auroral and non-auroral ionospheres display diffuse echoes indicative of ionospheric irregularities. These observations highlight the complexity of sources, transport, and dynamics of the Martian nightside ionosphere and suggest that a successful model of the nightside ionosphere would need to include both electron impact ionization and day-to-night plasma transport, the former of which can vary on short time and small spatial scales resulting from the highly dynamic magnetotail of Mars.

Abbreviations

EMM	Emirates Mars Mission
EMUS	Emirates Mars Ultraviolet Spectrometer
FUV	Far ultraviolet
IMF	Interplanetary magnetic field
MARSIS	Mars Advanced Radar for Subsurface and Ionosphere Sounding
MAVEN	Mars Atmosphere and Volatile Evolution
MEX	Mars Express

Acknowledgements

We thank the participants of the SWCMA2023 workshop (https://pat.gp.tohoku.ac.jp/ws/swcma2023/) for a fruitful discussion on discrete aurora at Mars.

Author contributions

YH and YF (KU) conceptualized the study and performed the data analysis. YH wrote the original draft. RJL and JD contributed to the acquisition and curation of EMM EMUS data. RJL, JD, and HN contributed to the interpretation of EMM EMUS data. BSC and ML contributed to the acquisition, curation, and interpretation of MEX MARSIS data. YF (IRF), MH, and RAF contributed to the acquisition, curation, and interpretation of MEX ASPERA-3 ELS data. All authors read and approved the final manuscript.

Funding

YH is supported by JSPS KAKENHI Grant (22K14085, 22H01285). B.S.-C. acknowledges support through UK-STFC Ernest Rutherford Fellowship ST/V004115/1. ML is funded by STFC grant ST/W00089X/1 and ESA contract ESA RFP/3-17233/21/ES/JD. The ESA contract also supported the MARSIS data processing.

Availability of data and materials

The EMM EMUS data used in this study are available in the EMM Science Data Center repository (https://sdc.emiratesmarsmission.ae/data/emus). The MEX MARSIS and ASPERA-3 data used in this study will become available in the ESA PSA archive (https://www.cosmos.esa.int/web/psa/mars-express).

Declarations

Competing interests

Not applicable.

Author details
[1]Department of Geophysics, Graduate School of Science, Kyoto University, Kyoto, Japan. [2]Space Sciences Laboratory, University of California Berkeley, Berkeley, CA, USA. [3]Laboratory for Atmospheric and Space Physics, University of Colorado, Boulder, CO, USA. [4]Graduate School of Science, Tohoku University, Sendai, Japan. [5]School of Physics and Astronomy, University of Leicester, Leicester, UK. [6]Swedish Institute of Space Physics, Kiruna, Sweden. [7]Southwest Research Institute, San Antonio, TX, USA.

Received: 13 February 2024 Accepted: 15 April 2024
Published online: 06 May 2024

References

Acuña MH, Connerney JEP, Ness NF, Lin RP, Mitchell D, Carlson CW, McFadden J, Anderson KA, Rème H (1999) Global distribution of crustal magnetization discovered by the mars global surveyor MAG/ER experiment. Science 284(5415):790–793. https://doi.org/10.1126/science.284.5415.790

Adams D, Xu S, Mitchell DL, Lillis RJ, Fillingim M, Andersson L, Fowler C, Connerney JEP, Espley J, Mazelle C (2018) Using magnetic topology to probe the sources of mars' nightside ionosphere. Geophys Res Lett 45(22):12190–12197. https://doi.org/10.1029/2018GL080629

Akalin F, Morgan D, Gurnett D, Kirchner D, Brain D, Modolo R, Acuña M, Espley J (2010) Dayside induced magnetic field in the ionosphere of Mars. Icarus 206(1):104–111. https://doi.org/10.1016/j.icarus.2009.03.021

Barabash S, Lundin R, Andersson H, Brinkfeldt K, Grigoriev A, Gunell H, Holmström M, Yamauchi M, Asamura K, Bochsler P, Wurz P, Cerulli-Irelli R, Mura A, Milillo A, Maggi M, Orsini S, Coates A, Linder D, Kataria D, Curtis C, Hsieh K, Sandel B, Frahm R, Sharber J, Winningham J, Grande M, Kallio E, Koskinen H, Riihelä P, Schmidt W, Säles T, Kozyra J, Krupp N, Woch J, Livi S, Luhmann J, McKenna-Lawlor S, Roelof E, Williams D, Sauvaud J-A, Fedorov A, Thocaven J-J (2006) The analyzer of space plasmas and energetic atoms (ASPERA-3) for the mars express mission. Space Sci Rev 126(1–4):113–164. https://doi.org/10.1007/s11214-006-9124-8

Bertaux J, Leblanc F, Witasse O, Quemerais E, Lilensten J, Stern S, Sandel B, Korablev O (2005) Discovery of an aurora on mars. Nature 435(7043):790–794. https://doi.org/10.1038/nature03603

Bowers CF, DiBraccio GA, Slavin JA, Johnston B, Schneider NM, Brain DA, Azari A (2023) Evidence for magnetic reconnection as the precursor to discrete aurora at mars. J Geophys Res 128(12):e2023JA031,622. https://doi.org/10.1029/2023JA031622

Bowers CF, DiBraccio GA, Slavin JA, Gruesbeck JR, Weber T, Xu S, Romanelli N, Harada Y (2023) Exploring the solar wind-planetary interaction at mars: implication for magnetic reconnection. J Geophys Res 128(2):e2022JA030,989. https://doi.org/10.1029/2022JA030989

Brain DA, Halekas JS (2013) Aurora in martian mini magnetospheres. Geophys Monogr Ser 197:123–132. https://doi.org/10.1029/2011GM001201

Brain DA, Halekas JS, Peticolas LM, Lin RP, Luhmann JG, Mitchell DL, Delory GT, Bougher SW, Acuña MH, Reme H (2006) On the origin of aurorae on Mars. Geophys Res Lett 33(1):L01, 201. https://doi.org/10.1029/2005GL024782

Brain DA, Lillis RJ, Mitchell DL, Halekas JS, Lin RP (2007) Electron pitch angle distributions as indicators of magnetic field topology near Mars. J Geophys Res 112(A9):A09, 201. https://doi.org/10.1029/2007JA012435

Cartacci M, Amata E, Cicchetti A, Noschese R, Giuppi S, Langlais B, Frigeri A, Orosei R, Picardi G (2013) Mars ionosphere total electron content analysis from marsis subsurface data. Icarus 223(1):423–437. https://doi.org/10.1016/j.icarus.2012.12.011

Chaffin MS, Fowler CM, Deighan J, Jain S, Holsclaw G, Hughes A, Ramstad R, Dong Y, Brain D, AlMazmi H, Chirakkil K, Correira J, England S, Evans JS, Fillingim M, Lillis R, Lootah F, Raghuram S, McFadden J, Halekas J, Espley J, Schneider N, Mayyasi M, Lee CO, Curry S, AlMatroushi H (2022) Patchy proton aurora at mars: a global view of solar wind precipitation across the martian dayside from emm/emus. Geophy Res Lett 49(17):e2022GL099,881. https://doi.org/10.1029/2022GL099881

Cui J, Cao Y-T, Wu X-S, Xu S-S, Yelle RV, Stone S, Vigren E, Edberg NJT, Shen C-L, He F, Wei Y (2019) Evaluating local ionization balance in the nightside martian upper atmosphere during maven deep dip campaigns. Astrophys J Lett 876(1):L12. https://doi.org/10.3847/2041-8213/ab1b34

Deighan J, Jain SK, Chaffin MS, Fang X, Halekas JS, Clarke JT, Schneider NM, Stewart AIF, Chaufray J-Y, Evans JS, Stevens MH, Mayyasi M, Stiepen A, Crismani M, McClintock WE, Holsclaw GM, Lo DY, Montmessin F, Lefèvre F, Jakosky BM (2018) Discovery of a proton aurora at Mars. Nat Astron 2(10):802–807. https://doi.org/10.1038/s41550-018-0538-5

DiBraccio GA, Espley JR, Gruesbeck JR, Connerney JEP, Brain DA, Halekas JS, Mitchell DL, McFadden JP, Harada Y, Livi R, Collinson G, Hara T, Mazelle C, Jakosky BM (2015) Magnetotail dynamics at Mars: initial MAVEN observations. Geophys Res Lett. https://doi.org/10.1002/2015GL065248

DiBraccio GA, Dann J, Espley JR, Gruesbeck JR, Soobiah Y, Connerney JEP, Halekas JS, Harada Y, Bowers CF, Brain DA, Ruhunusiri S, Hara T, Jakosky BM (2017) MAVEN observations of tail current sheet flapping at Mars. J Geophys Res 122(4):4308–4324. https://doi.org/10.1002/2016JA023488

Diéval C, Morgan DD, Němec F, Gurnett DA (2014) MARSIS observations of the Martian nightside ionosphere dependence on solar wind conditions. J Geophys Res 119(5):4077–4093. https://doi.org/10.1002/2014JA019788

Dong Y, Fang X, Brain DA, Hurley DM, Halekas JS, Espley JR, Ramstad R, Ruhunusiri S, Jakosky BM (2019) Magnetic field in the Martian Magnetosheath and the application as an IMF clock angle proxy. J Geophys Res 124(6):4295–4313. https://doi.org/10.1029/2019JA026522

Dubinin E, Fraenz M (2015) Magnetotails of Mars and Venus. Geophys Monogr Ser 207:43–59. https://doi.org/10.1002/9781118842324.ch3

Duru F, Morgan DD, Gurnett DA (2010) Overlapping ionospheric and surface echoes observed by the Mars express radar sounder near the Martian terminator. Geophys Res Lett 37(23):L23, 102. https://doi.org/10.1029/2010GL045859

Duru F, Gurnett DA, Morgan DD, Winningham JD, Frahm RA, Nagy AF (2011) Nightside ionosphere of Mars studied with local electron densities: a general overview and electron density depressions. J Geophys Res 116(A10):316. https://doi.org/10.1029/2011JA016835

Eastwood JP, Brain DA, Halekas JS, Drake JF, Phan TD, Oieroset M, Mitchell DL, Lin RP, Acuña M (2008) Evidence for collisionless magnetic reconnection at Mars. Geophys Res Lett 35(2):L02, 106. https://doi.org/10.1029/2007GL032289

Eastwood JP, Videira JJH, Brain DA, Halekas JS (2012) A chain of magnetic flux ropes in the magnetotail of Mars. Geophys Res Lett 39(3):L03, 104. https://doi.org/10.1029/2011GL050444

Espley JR, Cloutier PA, Brain DA, Crider DH, Acuña MH (2004) Observations of low-frequency magnetic oscillations in the Martian Magnetosheath, magnetic pileup region, and tail. J Geophys Res 109(A07):213. https://doi.org/10.1029/2003JA010193

Espley JR, Cloutier PA, Crider DH, Brain DA, Acuña MH (2005) Low-frequency plasma oscillations at mars during the october 2003 solar storm. J Geophys Res Space Phys 110(A9):A09S33. https://doi.org/10.1029/2004JA010935

Fillingim MO, Peticolas LM, Lillis RJ, Brain DA, Halekas JS, Mitchell DL, Lin RP, Lummerzheim D, Bougher SW, Kirchner DL (2007) Model calculations of electron precipitation induced ionization patches on the nightside of Mars. Geophys Res Lett 34(12):L12, 101. https://doi.org/10.1029/2007GL029986

Fowler CM, Andersson L, Ergun RE, Morooka M, Delory G, Andrews DJ, Lillis RJ, McEnulty T, Weber TD, Chamandy TM, Eriksson AI, Mitchell DL, Mazelle C, Jakosky BM (2015) The first in situ electron temperature and density measurements of the Martian nightside ionosphere. Geophys Res Lett 42(21):8854–8861. https://doi.org/10.1002/2015GL065267

Fowler CM, Hanley KG, McFadden JP, Chaston CC, Bonnell JW, Halekas JS, Espley JR, DiBraccio GA, Schwartz SJ, Mazelle C, Mitchell DL, Xu S, Lillis RJ (2021) Maven observations of low frequency steepened magnetosonic waves and associated heating of the martian nightside ionosphere. J Geophys Res Space Phys 126(10):e2021JA029,615. https://doi.org/10.1029/2021JA029615

Fox JL, Brannon JF, Porter HS (1993) Upper limits to the nightside ionosphere of mars. Geophys Res Lett 20(13):1339–1342. https://doi.org/10.1029/93GL01349

Gérard JC, Soret L, Libert L, Lundin R, Stiepen A, Radioti A, Bertaux JL (2015) Concurrent observations of ultraviolet aurora and energetic electron precipitation with Mars Express. J Geophys Res Space Phys 120(8):6749–6765. https://doi.org/10.1002/2015JA021150

Girazian Z, Mahaffy P, Lillis RJ, Benna M, Elrod M, Fowler CM, Mitchell DL (2017) Ion densities in the nightside ionosphere of mars: effects of electron impact ionization. Geophys Res Lett 44:11248–11256. https://doi.org/10.1002/2017GL075431

Girazian Z, Mahaffy PR, Lillis RJ, Benna M, Elrod M, Jakosky BM (2017) Nightside ionosphere of Mars: composition, vertical structure, and variability. J Geophys Res 122(4):4712–4725. https://doi.org/10.1002/2016JA023508
Girazian Z, Schneider NM, Milby Z, Fang X, Halekas J, Weber T, Jain SK, Gérard J-C, Soret L, Deighan J, Lee CO (2022) Discrete aurora at mars: dependence on upstream solar wind conditions. J Geophys Res Space Phys 127(4):e2021JA030,238. https://doi.org/10.1029/2021JA030238
Girazian Z, Halekas J, Lillis R (2021) Solar cycle and seasonal variability of the nightside ionosphere of mars: Insights from five years of maven observations, Icarus, p. 114615, https://doi.org/10.1016/j.icarus.2021.114615
Gurnett D, Huff R, Morgan D, Persoon A, Averkamp T, Kirchner D, Duru F, Akalin F, Kopf A, Nielsen E, Safaeinili A, Plaut J, Picardi G (2008) An overview of radar soundings of the martian ionosphere from the Mars Express spacecraft. Adv Space Res 41(9):1335–1346. https://doi.org/10.1016/j.asr.2007.01.062
Halekas JS, Luhmann JG, Dubinin E, Ma Y (2021) Induced magnetospheres, chap. 25, pp. 391–406, American Geophysical Union (AGU), https://doi.org/10.1002/9781119815624.ch25
Halekas JS, Eastwood JP, Brain DA, Phan TD, Oieroset M, Lin RP (2009) In situ observations of reconnection hall magnetic fields at mars: evidence for ion diffusion region encounters. J Geophys Res 114(A11):204. https://doi.org/10.1029/2009JA014544
Halekas JS, McFadden JP, Connerney JEP, Espley JR, Brain DA, Mitchell DL, Larson DE, Harada Y, Hara T, Ruhunusiri S, Jakosky BM (2015) Time-dispersed ion signatures observed in the Martian magnetosphere by MAVEN. Geophys Res Lett. https://doi.org/10.1002/2015GL064781
Hara T, Harada Y, Mitchell DL, DiBraccio GA, Espley JR, Brain DA, Halekas JS, Seki K, Luhmann JG, McFadden JP, Mazelle C, Jakosky BM (2017) On the origins of magnetic flux ropes in near-Mars magnetotail current sheets. Geophys Res Lett 44(15):7653–7662. https://doi.org/10.1002/2017GL073754
Harada Y, Halekas JS, McFadden JP, Mitchell DL, Mazelle C, Connerney JEP, Espley J, Larson DE, Brain DA, Andersson L, DiBraccio GA, Collinson GA, Livi R, Hara T, Ruhunusiri S, Jakosky BM (2015) Magnetic reconnection in the near-Mars magnetotail: MAVEN observations. Geophys Res Lett 42:8838–8845. https://doi.org/10.1002/2015GL065004
Harada Y, Mitchell DL, Halekas JS, McFadden JP, Mazelle C, Connerney JEP, Espley J, Brain DA, Larson DE, Lillis RJ, Hara T, Livi R, DiBraccio GA, Ruhunusiri S, Jakosky BM (2016) MAVEN observations of energy-time dispersed electron signatures in Martian crustal magnetic fields. Geophys Res Lett 43(3):939–944. https://doi.org/10.1002/2015GL067040
Harada Y, Andersson L, Fowler CM, Mitchell DL, Halekas JS, Mazelle C, Espley J, DiBraccio GA, McFadden JP, Brain DA, Xu S, Ruhunusiri S, Larson DE, Lillis RJ, Hara T, Livi R, Jakosky BM (2016) MAVEN observations of electron-induced whistler mode waves in the Martian magnetosphere. J Geophys Res. https://doi.org/10.1002/2016JA023194
Harada Y, Halekas JS, McFadden JP, Espley J, DiBraccio GA, Mitchell DL, Mazelle C, Brain DA, Andersson L, Ma YJ, Larson DE, Xu S, Hara T, Ruhunusiri S, Livi R, Jakosky BM (2017) Survey of magnetic reconnection signatures in the Martian magnetotail with MAVEN. J Geophys Res. https://doi.org/10.1002/2017JA023952
Harada Y, Gurnett DA, Kopf AJ, Halekas JS, Ruhunusiri S, DiBraccio GA, Espley J, Brain DA (2018) MARSIS observations of the martian nightside ionosphere during the september 2017 solar event. Geophys Res Lett 45(16):7960–7967. https://doi.org/10.1002/2018GL077622
Harada Y, Gurnett DA, Kopf AJ, Halekas JS, Ruhunusiri S (2018) Ionospheric irregularities at mars probed by MARSIS topside sounding. J Geophys Res. https://doi.org/10.1002/2017JA024913
Harada Y, Ruhunusiri S, Halekas JS, Espley J, DiBraccio GA, Mcfadden JP, Mitchell DL, Mazelle C, Collinson G, Brain DA, Hara T, Nosé M, Oimatsu S, Yamamoto K, Jakosky BM (2019) Locally generated ulf waves in the martian magnetosphere: Maven observations. J Geophys Res Space Phys 124(11):8707–8726. https://doi.org/10.1029/2019JA027312
Harada Y, Halekas JS, Xu S, DiBraccio GA, Ruhunusiri S, Hara T, Mcfadden JP, Espley JR, Mitchell DL, Mazelle C (2020) Ion jets within current sheets in the martian magnetosphere. J Geophys Res Space Phys 125(12):e2020JA028,576. https://doi.org/10.1029/2020JA028576
Johnston BJ, Schneider NM, Jain SK, Milby Z, Deighan J, Bowers CF, DiBraccio GA, Gérard J-C, Soret L, Girazian Z, Brain DA, Ruhunusiri S, Curry S (2023) Discrete aurora at mars: insights into the role of magnetic reconnection. Geophs Res Lett 50(24):e2023GL104,198. https://doi.org/10.1029/2023GL104198
Leblanc F, Witasse O, Winningham J, Brain D, Lilensten J, Blelly PL, Frahm RA, Halekas JS, Bertaux JL (2006) Origins of the Martian aurora observed by spectroscopy for investigation of characteristics of the atmosphere of Mars (SPICAM) on board mars express. J Geophys Res 111(A9):A09, 313. https://doi.org/10.1029/2006JA011763
Leblanc F, Witasse O, Lilensten J, Frahm RA, Safaenili A, Brain DA, Mouginot J, Nilsson H, Futaana Y, Halekas J, Holmström M, Bertaux JL, Winningham JD, Kofman W, Lundin R (2008) Observations of aurorae by SPICAM ultraviolet spectrograph on board mars express: simultaneous ASPERA-3 and MARSIS measurements. J Geophys Res 113(A8):A08, 311. https://doi.org/10.1029/2008JA013033
Lester M, Sanchez-Cano B, Potts D, Lillis R, Cartacci M, Bernardini F, Orosei R, Perry M, Putzig N, Campbell B, Blelly P-L, Milan S, Opgenoorth H, Witasse O, Redrojo EMM, Russell A (2022) The impact of energetic particles on the martian ionosphere during a full solar cycle of radar observations: radar blackouts. J Geophys Res Space Phys 127(2):e2021JA029,535. https://doi.org/10.1029/2021JA029535
Lillis RJ, Fillingim MO, Peticolas LM, Brain DA, Lin RP, Bougher SW (2009) Nightside ionosphere of Mars: modeling the effects of crustal magnetic fields and electron pitch angle distributions on electron impact ionization. J Geophys Res 114(E11):E11, 009. https://doi.org/10.1029/2009JE003379
Lillis RJ, Deighan J, Brain D, Fillingim M, Jain S, Chaffin M, England S, Holsclaw G, Chirakkil K, Al Matroushi H, Lootah F, Al Mazmi H, Thiemann E, Eparvier F, Schneider N, Curry S (2022) First synoptic images of fuv discrete aurora and discovery of sinuous aurora at mars by emm emus. Geophys Res Lett 49(16):e2022GL099,820. https://doi.org/10.1029/2022GL099820
Mayyasi M, Narvaez C, Benna M, Elrod M, Mahaffy P (2019) Ion-neutral coupling in the upper atmosphere of mars: a dominant driver of topside ionospheric structure. J Geophys Res Space Phys 124(5):3786–3798. https://doi.org/10.1029/2019JA026481
Mitchell D, Lin R, Mazelle C, Reme H, Cloutier P, Connerney J, Acuña M, Ness N (2001) Probing Mars' crustal magnetic field and ionosphere with the MGS electron reflectometer. J Geophys Res 106(E10):23419–23427. https://doi.org/10.1029/2000JE001435
Morschhauser A, Lesur V, Grott M (2014) A spherical harmonic model of the lithospheric magnetic field of Mars. J Geophys Res 119(6):1162–1188. https://doi.org/10.1002/2013JE004555
Němec F, Morgan DD, Gurnett DA, Duru F (2010) Nightside ionosphere of Mars: radar soundings by the mars express spacecraft. J Geophys Res 115(E12):E12, 009. https://doi.org/10.1029/2010JE003663
Němec F, Morgan DD, Gurnett DA, Brain DA (2011) Areas of enhanced ionization in the deep nightside ionosphere of Mars. J Geophys Res 116(E6):E06,006. https://doi.org/10.1029/2011JE003804
Němec F, Morgan DD, Diéval C, Gurnett DA, Futaana Y (2014) Enhanced ionization of the Martian nightside ionosphere during solar energetic particle events. Geophys Res Lett 41(3):793–798. https://doi.org/10.1002/2013GL058895
Park J (2024) Climatology of martian ionospheric disturbances deduced from maven data in 2014–2023. J Geophys Res Space Phys 129(1):e2023JA031,991. https://doi.org/10.1029/2023JA031991
Qin J, Zou H, Futaana Y, Ye Y, Hao Y, Nielsen E, Wang J (2021) Double-peak structures of martian nightside total electron content in strong crustal magnetic cusp regions. Geophys Res Lett 48(7):e2021GL092,662. https://doi.org/10.1029/2021GL092662
Qin J, Zou H, Ye Y, Hao Y, Wang J (2022) A denser and elevated martian nightside ionosphere during mars season ls 180–360°. Icarus 388(115):255. https://doi.org/10.1016/j.icarus.2022.115255
Ritter B, Gérard JC, Hubert B, Rodriguez L, Montmessin F (2018) Observations of the proton Aurora on Mars With SPICAM on board mars express. Geophys Res Lett 45(2):612–619. https://doi.org/10.1002/2017GL076235
Ruhunusiri S, Halekas JS, Connerney JEP, Espley JR, McFadden JP, Larson DE, Mitchell DL, Mazelle C, Jakosky BM (2015) Low frequency waves in the Martian magnetosphere and their response to upstream solar wind driving conditions. Geophys Res Lett. https://doi.org/10.1002/2015GL064968
Safaeinili A, Kofman W, Mouginot J, Gim Y, Herique A, Ivanov AB, Plaut JJ, Picardi G (2007) Estimation of the total electron content of the martian ionosphere using radar sounder surface echoes. Geophys Res Lett. https://doi.org/10.1029/2007GL032154
Schneider NM, Deighan JI, Jain SK, Stiepen A, Stewart AIF, Larson D, Mitchell DL, Mazelle C, Lee CO, Lillis RJ, Evans JS, Brain D, Stevens MH, McClintock WE, Chaffin MS, Crismani M, Holsclaw GM, Lefevre F, Lo DY, Clarke JT,

Montmessin F, Jakosky BM (2015) Discovery of diffuse aurora on Mars. Science. https://doi.org/10.1126/science.aad0313
Schneider NM, Jain SK, Deighan J, Nasr CR, Brain DA, Larson D, Lillis R, Rahmati A, Halekas JS, Lee CO, Chaffin MS, Stiepen A, Crismani M, Evans JS, Stevens MH, Lo DY, McClintock WE, Stewart AIF, Yelle RV, Clarke JT, Holsclaw GM, Lefevre F, Montmessin F, Jakosky BM (2018) Global Aurora on Mars during the september 2017 space weather event. Geophys Res Lett 45(15):7391–7398. https://doi.org/10.1029/2018GL077772
Schneider NM, Milby Z, Jain SK, Gérard J-C, Soret L, Brain DA, Weber T, Girazian Z, McFadden J, Deighan J, Jakosky BM (2021) Discrete aurora on mars: insights into their distribution and activity from maven/iuvs observations. J Geophys Res Space Phys 126(10):e2021JA029,428. https://doi.org/10.1029/2021JA029428
Soret L, Gérard J-C, Libert L, Shematovich VI, Bisikalo DV, Stiepen A, Bertaux J-L (2016) Spicam observations and modeling of mars aurorae. Icarus 264:398–406. https://doi.org/10.1016/j.icarus.2015.09.023
Soret L, Gérard J-C, Schneider N, Jain S, Milby Z, Ritter B, Hubert B, Weber T (2021) Discrete aurora on mars: spectral properties, vertical profiles, and electron energies. J Geophys Res Space Phys 126(10):e2021JA029,495. https://doi.org/10.1029/2021JA029495
Steckiewicz M, Mazelle C, Garnier P, André N, Penou E, Beth A, Sauvaud J-A, Toublanc D, Mitchell DL, McFadden JP, Luhmann JG, Lillis RJ, Connerney JEP, Espley JR, Andersson L, Halekas JS, Larson DE, Jakosky BM (2015) Altitude dependence of nightside Martian suprathermal electron depletions as revealed by MAVEN observations. Geophys Res Lett 42(21):8877–8884. https://doi.org/10.1002/2015GL065257
Teng S, Wu Y, Harada Y, Bortnik J, Zonca F, Chen L, Tao X (2023) Whistler-mode chorus waves at mars. Nat Commun 14(1):3142. https://doi.org/10.1038/s41467-023-38776-z
Wang L, Huang C, Du A, Ge Y, Chen G, Fan J, Qin J (2023) Magnetic reconnection in the martian magnetotail: occurrence rate and impact on ion loss. Geophys Res Lett 50(18):e2023GL104,996. https://doi.org/10.1029/2023GL104996
Withers P (2009) A review of observed variability in the dayside ionosphere of Mars. Adv Space Res 44(3):277–307. https://doi.org/10.1016/j.asr.2009.04.027
Withers P, Fillingim MO, Lillis RJ, Häusler B, Hinson DP, Tyler GL, Pätzold M, Peter K, Tellmann S, Witasse O (2012) Observations of the nightside ionosphere of Mars by the Mars express radio science experiment (MaRS). J Geophys Res 117(A12):A12, 307. https://doi.org/10.1029/2012JA018185
Xu S, Mitchell DL, McFadden JP, Fillingim MO, Andersson L, Brain DA, Weber T, Schneider NM, Jain S, Fowler CM, Lillis R, Mazelle C, Espley J (2020) Inverted-v electron acceleration events concurring with localized auroral observations at mars by maven. Geophys Res Lett 47(9):e2020GL087,414. https://doi.org/10.1029/2020GL087414
Xu S, Mitchell DL, McFadden JP, Schneider NM, Milby Z, Jain S, Weber T, Brain DA, DiBraccio GA, Halekas J, Ruhunusiri S, Mazelle C, Lillis RJ, Johnston B (2022) Empirically determined auroral electron events at mars–maven observations. Geophys Res Lett 49(6):e2022GL097,757. https://doi.org/10.1029/2022GL097757
Xu S, Mitchell DL, McFadden JP, Fowler CM, Hanley K, Weber T, Brain DA, DiBraccio GA, Liemohn MW, Lillis RJ, Halekas JS, Ruhunusiri S, Andersson L, Mazelle C, Curry SM (2022) Nightside auroral electrons at mars: upstream drivers and ionospheric impact. J Geophys Res Space Phys 127(9):e2022JA030,801. https://doi.org/10.1029/2022JA030801
Zhang C, Nilsson H, Ebihara Y, Yamauchi M, Persson M, Rong Z, Zhong J, Dong C, Chen Y, Zhou X, Sun Y, Harada Y, Halekas J, Xu S, Futaana Y, Shi Z, Yuan C, Yun X, Fu S, Gao J, Holmström M, Wei Y, Barabash S (2023) Detection of magnetospheric ion drift patterns at mars. Nat Commun 14(1):6866. https://doi.org/10.1038/s41467-023-42630-7
Zhang C, Rong Z, Zhang L, Gao J, Shi Z, Klinger L, Shen C, Wei Y (2023) Properties of flapping current sheet of the martian magnetotail. J Geophys Res Space Phys 128(4):e2022JA031,232. https://doi.org/10.1029/2022JA031232

Publisher's Note